AIAA 92-0321

Euler Calculations of Axisymmetric Under-Expanded Jets by an Adaptive-Refinement Method

D. De Zeeuw and K. G. Powell
Department of Aerospace Engineering
The University of Michigan
Ann Arbor, MI USA

30th Aerospace Sciences Meeting & Exhibit
January 6-9, 1992 / Reno, NV

Euler Calculations of Axisymmetric Under-Expanded Jets by an Adaptive-Refinement Method

Darren De Zeeuw *
Kenneth G. Powell †

The University of Michigan
Department of Aerospace Engineering
Ann Arbor, MI 48109-2140

January, 1992

Abstract

Under-expanded jet flows are calculated using an adaptive-refinement solution method for the axisymmetric Euler equations. The solution procedure is tree-based, and flux-vector splitting and a positive, linear reconstruction method are used. The refinement criterion, based on the divergence and curl of the local velocity, is shown to capture the flow features adequately. Results are presented for a range of jet-to-stream total pressure ratios, and for two jet Mach numbers. The resulting flows show a complex shock-shear-expansion structure, with Mach disks forming at high jet-to-stream pressure ratios. The location of the Mach disk is shown to be sensitive to the jet Mach number.

1 Introduction

Even at relatively low altitudes, rocket exhaust jets are typically under-expanded. The structure of such under-expanded jet flows is rich, typically being comprised of:

- an external shock emanating from near the lip of the nozzle;
- a shear at the jet boundary;
- an expansion fan emanating from the lip of the nozzle;
- an intercepting shock emanating from the lip of the nozzle;
- a reflection of the intercepting shock;

and, for very low back pressures:

- a Mach disc;
- a slip line emanating from the intersection point of the intercepting shock and the Mach disc.

This structure, for an axisymmetric jet, is diagrammed in Figure 1.

Due to the highly nonlinear nature of these flows, the Euler equations are the lowest order of approximation that gives a reasonable model for the fluid physics. The use of the Euler equations, rather than a higher-order model, is predicated on the assumptions that the Knudsen number is small, the Reynolds number large, and that there is negligible reaction in the jet flow. In general, these assumptions are relatively safe, except for the region near the jet boundary, where substantial mixing takes place [T. 64]. Effects of turbulent mixing, which can substantially alter the flow far downstream of the nozzle, are also neglected in this study.

*Doctoral Candidate, Member AIAA
†Assistant Professor, Senior Member AIAA

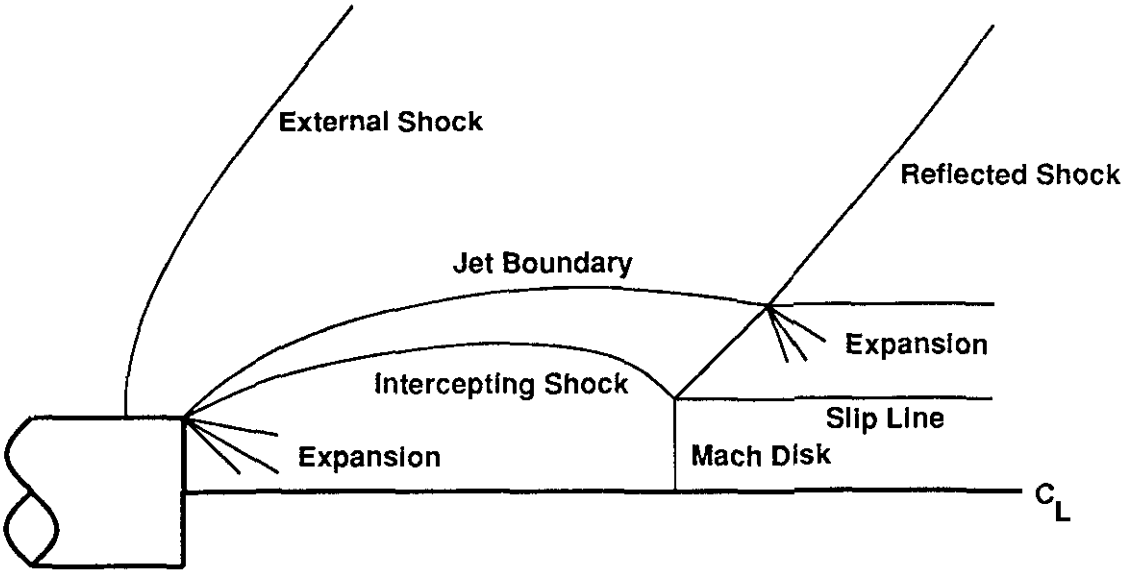

Figure 1: Schematic of an Under-Expanded Jet with Mach Disk

Since these flows exhibit high-gradient features whose geometry cannot be determined *a priori*, a solution-adaptive technique is necessary for obtaining high-fidelity solutions. An adaptive-refinement method [DP91, PPD92] is used, with cells being added in regions in which compressibility or rotationality are appreciable. The solution scheme is described below, along with numerical results for several jet flows.

2 Solution Technique

2.1 Data Structure

The basic data structure used is a cell-based tree structure — "parent" cells are refined by spawning four "children" cells. This concept is illustrated in Figure 2. Each cell has a pointer to its parent cell (if one exists) and to its four children cells (if they exist). The cells farthest down the hierarchy, that is, the ones with no children, are the cells on which the calculation takes place. This tree structure contains all the connectivity information necessary to carry out the flow calculations; no other connectivity information is stored. For instance, finding a neighbor cell requires, in the best case, simply querying the parent cell for the location of another of its children. In the worst case, the tree must be traversed all the way to its root. More generally, the expected number of levels of the tree that must be traversed to find a neighbor asymptotes to

$$\begin{aligned} E(n_{lev}) &= \frac{1}{2} + \frac{1}{2}\left(\frac{2}{2} + \frac{1}{2}\left(\frac{3}{2} \cdots\right.\right. \\ &= \sum \frac{k}{2^k} \\ &\asymp 2 \end{aligned}$$

i.e. the neighboring cell is typically a grandchild of the current cell's grandparent.

2.2 Generation of an Initial Mesh

The generation of the initial mesh begins with the creation of the "root" cell. Its size is determined from the size of the flow field and by what the user determines to be the coarsest acceptable mesh for that flow field. Then cells without children, initially just the root cell, are refined until the mesh reaches the coarsest acceptable mesh. This

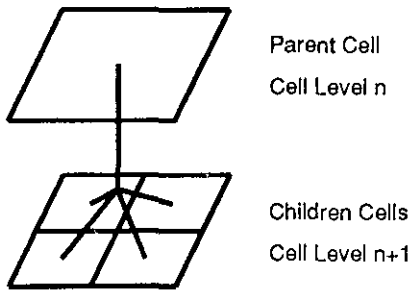

Figure 2: Parent/Children Relationship

mesh serves as the initial mesh for cases in which no body is cut out of the grid. A technique for assuring proper resolution of high-curvature regions of a body in a flow has been presented elsewhere [DP91].

2.3 Solution-Based Mesh Refinement

An adaptive mesh may be refined or coarsened based on the characteristics of the flow about the body. For steady-state calculations, refinement takes place only after a solution is sufficiently converged. At that point, cells are flagged for refinement based on two criteria. The first, based on the curl of the velocity vector, senses regions in which rotationality is appreciable. The second, based on the divergence of the velocity vector, senses regions in which compressibility is important. Cells are flagged for refinement if either type of region is detected; cells are flagged for coarsening if neither type of region is detected.

For each computational cell, the rotationality criterion, τ_r, and the compressibility criterion, τ_c, are calculated. Then the standard deviation about zero for both criteria, σ_r and σ_c, are calculated using only those cells which have a length scale $L > L_{min}$, where L_{min} is a minimum allowable cell size. Thus, if a cell is already at its smallest allowable size, it will not be used in determining the standard deviations of the adaptation criteria. The effect of this is that, once a flow feature has been resolved, the refinement will look for other, weaker features to resolve. The cell may, however, be flagged for coarsening, since the flow feature that was once there may have moved or disappeared. Cells that have a length scale $L > L_{min}$ are refined if either the rotationality or compressibility criterion lie more than one standard deviation away from zero, the value for uniform flow. Cells are flagged for coarsening if both the compressibility and rotationality criteria lie within one-tenth of a standard deviation from zero.

The standard deviations σ_r and σ_c are determined by

$$\tau_r = |\nabla \times \mathbf{U}| L^{\frac{3}{2}} \quad , \quad \sigma_r = \sqrt{\frac{\sum_{i=1}^{n} \tau_{r_i}^2}{n}}$$

$$\tau_c = |\nabla \cdot \mathbf{U}| L^{\frac{3}{2}} \quad , \quad \sigma_c = \sqrt{\frac{\sum_{i=1}^{n} \tau_{c_i}^2}{n}} \tag{1}$$

Cells are be flagged for refinement if

$$L > L_{min} \quad \text{and} \quad (|\tau_c| > \sigma_c \quad \text{or} \quad |\tau_r| > \sigma_r) \; ; \tag{2}$$

cells are flagged for coarsening if

$$|\tau_c| < \tfrac{\sigma_c}{10} \quad \text{and} \quad |\tau_r| < \tfrac{\sigma_r}{10} \; . \tag{3}$$

2.4 Reconstruction Procedure

In order to evaluate the flux through a face, flow quantities are required at both sides of the face. To achieve higher-order accuracy, solution-gradient information must be used. A linear reconstruction method [Bar90] is used to determine a second-order approximation to the state at the face midpoint, based on the cells in the neighborhood of the face. It relies on a suitable path integral about the cell of interest, with the gradient of a quantity W_k in a cell

being determined by

$$\nabla W_k = \frac{1}{A_\Omega} \int_{\partial\Omega} W_k \hat{\mathbf{n}} d\ell \,, \tag{4}$$

where A_Ω is the area enclosed by the path of integration, $\partial\Omega$. Here, W_k represents the quantity being reconstructed; in this work, the primitive variables $\mathbf{W} = (\rho, u, v, p)^T$ are reconstructed, to ensure positivity of density and pressure.

The path for the integration is constructed by connecting the centroids of neighboring cells. Away from cut cells or cell-level differences, the eight immediate neighbors of a cell are used. Near a body, as few as four cells are used to construct the path. For a linear reconstruction, a minimum of three non-collinear cell-centers are required to form a proper path. Some examples of the paths are shown in Figure 3 to the normal path, with the X denoting the cell for which the gradient is being calculated. For the calculations in this paper, the only cells that require one-sided paths are those that lie along the wall of the nozzle.

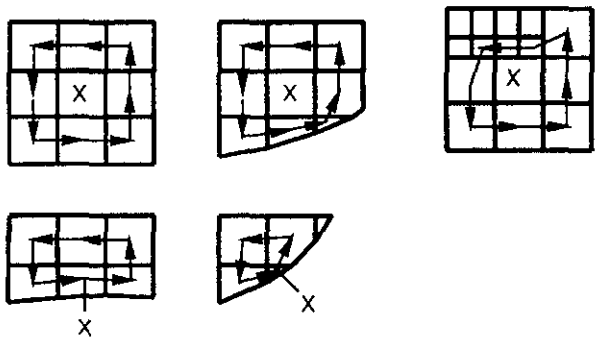

Figure 3: Normal And Special Paths

Once the cells in the path are determined, the path integral is carried out numerically. In general, the area inside the path is calculated by summing the areas of the triangles formed by connecting the centroids in the path to the centroid of the cell for which the gradient is being calculated. Once the gradient of W_k is known in each cell, the value of W_k can be found anywhere in the cell from

$$W_k(x, y) = W_k^c + \nabla W_k \cdot \mathbf{dr} \tag{5}$$

where W_k^c is the value of W_k at the cell centroid, and $\mathbf{dr}$ is defined as

$$dr_x = (x - x^c) \quad , \quad dr_y = (y - y^c) \quad . \tag{6}$$

2.5 Limiting

If the full gradient were used in reconstructing the values at face midpoints, the computed values could fall outside the bounds of the data used to determine the gradients. To avoid this, the computed gradients are *limited*; that is the primitive variables $\mathbf{W} = (\rho, u, v, p)^T$ are reconstructed via

$$\mathbf{W}(x, y) = \mathbf{W}^c + \phi \nabla \mathbf{W} \cdot \mathbf{dr} \tag{7}$$

where ϕ is a limiter, with a value between zero and one. In regions where $\phi = 1$, a piecewise-linear reconstruction is being used; in regions where $\phi = 0$, a piecewise-constant reconstruction is being used. The limiter ϕ is defined as

$$\phi = \min \begin{cases} 1 \\ \min_k \left(\frac{|W_k^c - \max_{neighbors}(W_k)|}{|W_k^c - \max_{cell}(W_k)|} \right) \\ \min_k \left(\frac{|W_k^c - \min_{neighbors}(W_k)|}{|W_k^c - \min_{cell}(W_k)|} \right) \end{cases} \quad . \tag{8}$$

The minimum and maximum over the neighbors are found by examining the values of W_k used to determine the gradients; the minimum and maximum over the cell are found by using the gradient to reconstruct W_k at the corners

of the cell. Thus, the limiter acts to ensure that the values of W_k at the nodes of the cell for which the gradient is being calculated are bounded by the values of W_k that are used in calculating the gradient. Using a single limiter for the gradient of the vector $\mathbf{W}$ was found to give better convergence and smoother results, at the cost of higher dissipation. In standard MUSCL-type schemes [vL79], a separate limiter is typically used for each variable, and for each mesh direction, resulting in eight limiters for each cell.

Unfortunately, limiting can seriously hamper the convergence to a steady state, with the nonlinearity of the scheme resulting in limit cycles. To combat this problem, the limiter values are "frozen" after a certain point in the convergence, using previously stored values of the limiter rather than recomputing them at each time step. Freezing the limiters allows the residuals to converge to machine zero.

2.6 Flux-Vector Splitting

The finite-volume form of the axisymmetric Euler equations can be written as

$$\frac{d\mathbf{U}}{dt} = -\frac{1}{A\bar{y}} \sum_{faces} (\mathbf{F}\Delta y - \mathbf{G}\Delta x) + \mathbf{S} \tag{9}$$

where A is the area of that cell, Δx and Δy are the changes of x and y along a face (defined so that the integral is carried out in a counter-clockwise sense), and $\mathbf{U}$, $\mathbf{F}$, $\mathbf{G}$ and $\mathbf{S}$ are defined as

$$\mathbf{U} = \begin{pmatrix} \rho \\ \rho u \\ \rho v \\ \rho E \end{pmatrix} , \quad \mathbf{F} = \begin{pmatrix} y\rho u \\ y\rho u^2 + yp \\ y\rho uv \\ y\rho uH \end{pmatrix} , \quad \mathbf{G} = \begin{pmatrix} y\rho v \\ y\rho vu \\ y\rho v^2 + yp \\ y\rho vH \end{pmatrix} , \quad \mathbf{S} = \begin{pmatrix} 0 \\ 0 \\ \frac{p}{y} \\ 0 \end{pmatrix} . \tag{10}$$

Defining the face length and the normal and tangential velocities as

$$\Delta s = \sqrt{(\Delta x)^2 + (\Delta y)^2} \tag{11}$$

and

$$u_n = \frac{(u\Delta y - v\Delta x)}{\Delta s} \qquad u_t = \frac{(u\Delta x + v\Delta y)}{\Delta s} , \tag{12}$$

the flux through a face may be written as

$$(\mathbf{F}\Delta y - \mathbf{G}\Delta x) \equiv \mathbf{\Phi}\Delta s . \tag{13}$$

The flux through a face is a function of the values at the face midpoint, given by the reconstruction in the cells to the "left" and "right" of the face. Using van Leer's flux vector splitting, $\mathbf{\Phi}$ is defined as

$$\mathbf{\Phi} = \mathbf{T}^{-1} \left(\mathbf{H}^+(\mathbf{U}_L) + \mathbf{H}^-(\mathbf{U}_R) \right) , \tag{14}$$

where

$$\mathbf{T} = \begin{pmatrix} 1 & 0 & 0 & 0 \\ 0 & \frac{\Delta y}{\Delta s} & -\frac{\Delta x}{\Delta s} & 0 \\ 0 & \frac{\Delta x}{\Delta s} & \frac{\Delta y}{\Delta s} & 0 \\ 0 & 0 & 0 & 1 \end{pmatrix} \quad \text{and} \quad \mathbf{H} = \begin{pmatrix} y\rho u_n \\ y\rho u_n^2 + yp \\ y\rho u_n u_t \\ y\rho u_n H \end{pmatrix} . \tag{15}$$

The split fluxes $\mathbf{H}^+$ and $\mathbf{H}^-$ are defined for various normal Mach numbers as

$$\begin{array}{rcll} M_n & \geq & 1 & \mathbf{H}^+ = \mathbf{H}, \mathbf{H}^- = 0 \\ M_n & \leq & -1 & \mathbf{H}^+ = 0, \mathbf{H}^- = \mathbf{H} \\ |M_n| & \leq & 1 & \mathbf{H}^\pm = \begin{pmatrix} h_1^\pm \\ h_2^\pm \\ h_3^\pm \\ h_4^\pm \end{pmatrix} = \begin{pmatrix} \pm y\rho c \left(M_n \pm 1\right)^2 / 4 \\ h_1^\pm c \left[\left(\gamma - 1\right) M_n \pm 2 \right] / \gamma \\ h_1^\pm c M_t \\ h_1^\pm c^2 \left[\left(\gamma - 1\right) M_n \pm 2 \right]^2 / \left[2\left(\gamma^2 - 1\right) + M_t^2 / 2 \right] \end{pmatrix} . \end{array} \tag{16}$$

For each cell, the face fluxes, calculated as above, are summed to give the residual for the cell,

$$\mathbf{Res}\,(\mathbf{U}) = -\frac{1}{A\bar{y}} \sum_{faces} \mathbf{\Phi}\ \Delta s + \mathbf{S} \tag{17}$$

These residuals are then integrated in time, as described below.

2.7 Time-Stepping Scheme

The time-stepping scheme used is one of the optimally-smoothing multi-stage schemes developed by Tai [Tai90, vLTP89]. The general m-stage scheme is defined as

$$\begin{aligned} \mathbf{U}^{(0)} &= \mathbf{U}^n \\ \mathbf{U}^{(k)} &= \mathbf{U}^{(0)} + \alpha_k \Delta t \mathbf{Res}\left(\mathbf{U}^{(k-1)}\right), k = 1, m \\ \mathbf{U}^{n+1} &= \mathbf{U}^{(m)}\,. \end{aligned} \tag{18}$$

The five-stage scheme which gives optimal damping of Fourier modes in the range $\pi/4 \leq k\Delta x \leq \pi$ has multi-stage coefficients

$$(\alpha_1, \alpha_2, \alpha_3, \alpha_4, \alpha_5) = (0.0695, 0.1602, 0.2898, 0.5060, 1.0000) \tag{19}$$

and CFL number 1.1508. Local time-stepping is used in the calculations.

2.8 Post-Processing

Post-processing requires transferring the known cell-centered values to nodal values for plotting as accurately as possible. To do this, the limited cell gradients are used to extrapolate to each cell's nodes as shown in Figure 4.

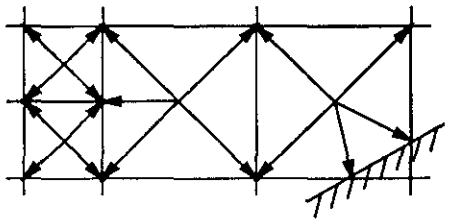

Figure 4: Obtaining Post-Processed Nodal Values

The function as reconstructed at the nodes is multi-valued; there is one value resulting from the representation in each cell sharing that node. These multiple values at each node are averaged to yield a single accurate, bounded value there.

3 Results For Axisymmetric Under-Expanded Jet Flows

The class of flows considered here can be characterized by:

- the Mach number of the stream;
- the Mach number of the jet;
- the jet-to-stream total pressure ratio p_{0_j}/p_{0_s};
- the jet-to-stream total temperature ratio T_{0_j}/T_{0_s}.

For all of the flows considered here, the total temperature ratio is taken to be unity. Four cases are considered:

1. $M_j = 1.25, M_s = 1.25, p_{0_j}/p_{0_s} = 20$;

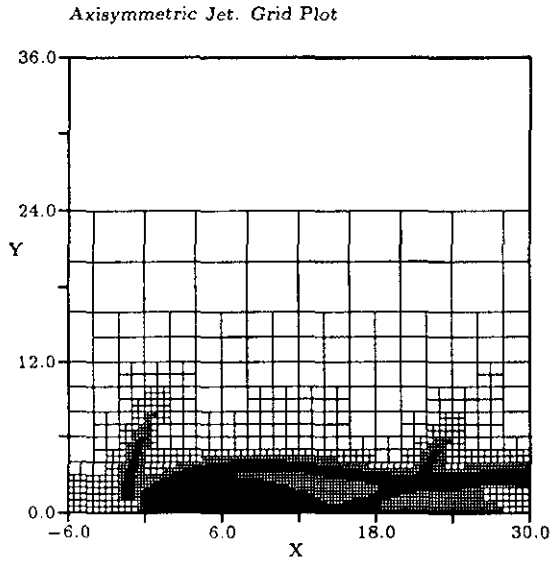

Figure 5: Mesh, $P_{0_{jet}}/P_{0_{stream}} = 20$, $M = 1.25$

2. $M_j = 1.25, M_s = 1.25, p_{0_j}/p_{0_s} = 5$;
3. $M_j = 1.25, M_s = 1.25, p_{0_j}/p_{0_s} = 50$;
4. $M_j = 1.05, M_s = 1.05, p_{0_j}/p_{0_s} = 50$;

3.1 Total Pressure Ratio of 20, M=1.25

Results for this case are shown in Figures 5–8. The final grid for the case is shown in Figure 5. The refinement criterion has detected the external shock, the intercepting shock and its reflection, the jet boundary, and the rapid expansion at the exit of the nozzle. Neither the pressure (Figure 6) nor the density (Figure 7) is affected by most of these features. In the density contours, the effect of the expansion dominates, and the reflected shock is visible, but the intercepting shock, the external shock and the jet boundary are nearly invisible. In the pressure contours, the results are similar, but the jet boundary is totally invisible, as the pressure is constant across this surface. All of the features are apparent in the Mach number contours (Figure 8).

3.2 Total Pressure Ratio of 5, M=1.25

This case, depicted in Figures 9 and 10, shows the effect of decreasing the total pressure ratio between the jet and the stream. The flow is qualitatively very similar to the previous case. The features are weaker, and closer to the nozzle exit. In particular, the intercepting shock does not form immediately at the lip of the nozzle; the characteristics from that point do not coalesce until very near the axis of symmetry. The reflection of the shock is much more apparent. The pressure and density contours for this case are not shown; as in the previous case, the expansion is the dominant feature apparent in those variables.

3.3 Total Pressure Ratio of 50, M=1.25

This case, depicted in Figures 11 and 12, shows the effect of increasing the total pressure ratio between jet and stream. At this higher pressure ratio, there is no longer a simple reflection of the intercepting shock from the axis; instead, a large Mach disk is formed. The slip line emanating from the top of the Mach disk is as apparent as the jet boundary in this case. Also, because of the lower pressure of the outer stream, the jet boundary is more highly curved, and acceleration of the outer flow as it follows the jet boundary is apparent in the Mach contours. The refinement criterion has again performed well, detecting all of the features of the flow.

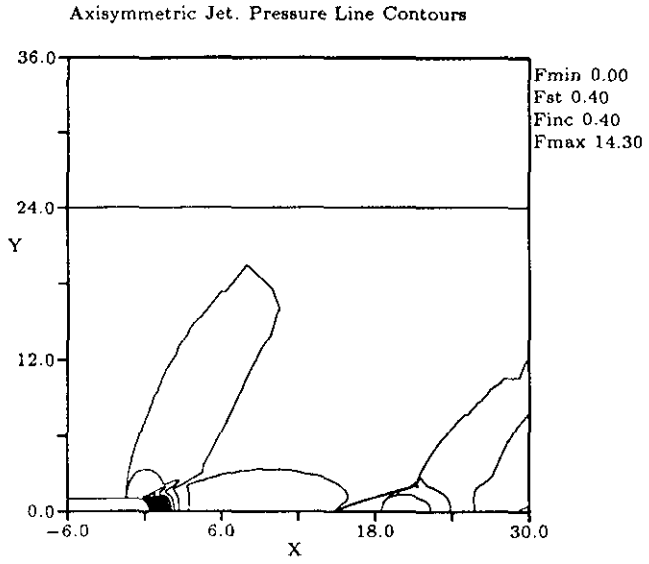

Figure 6: Pressure Contours, $P_{0_{jet}}/P_{0_{stream}} = 20$, $M = 1.25$

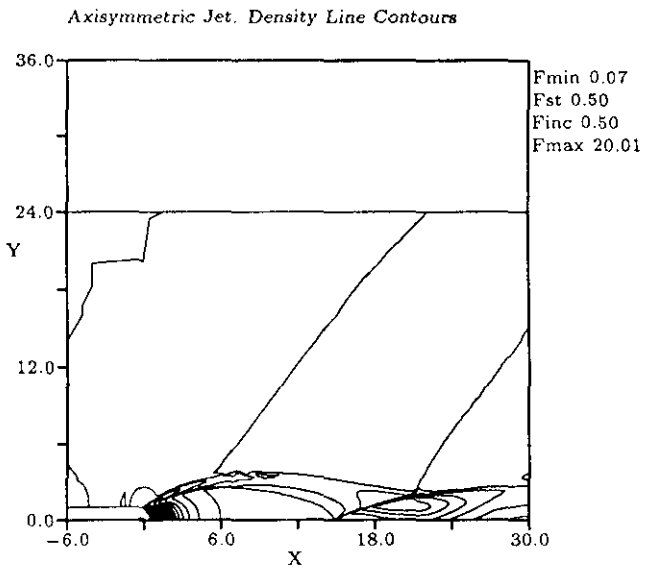

Figure 7: Density Contours, $P_{0_{jet}}/P_{0_{stream}} = 20$, $M = 1.25$

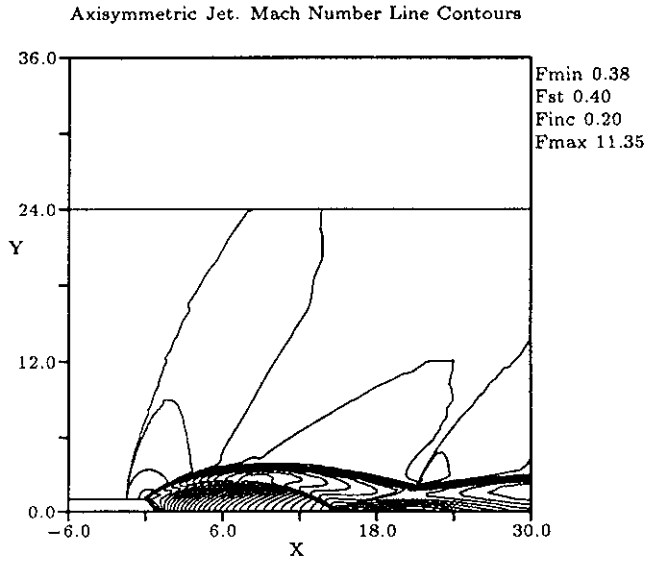

Figure 8: Mach Number Contours, $P_{0_{jet}}/P_{0_{stream}} = 20$, $M = 1.25$

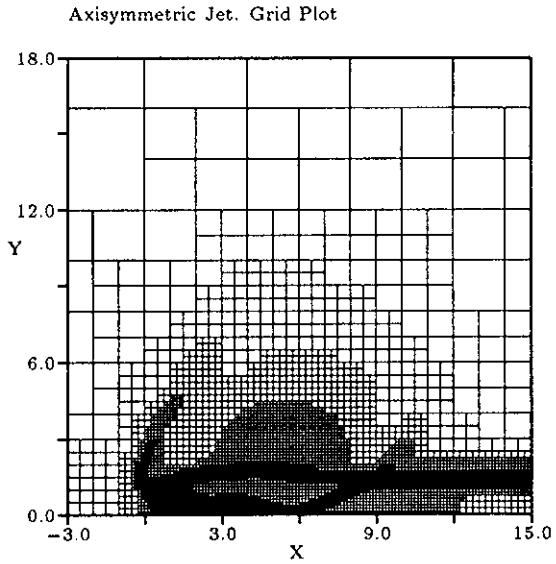

Figure 9: Mesh, $P_{0_{jet}}/P_{0_{stream}} = 5$, $M = 1.25$

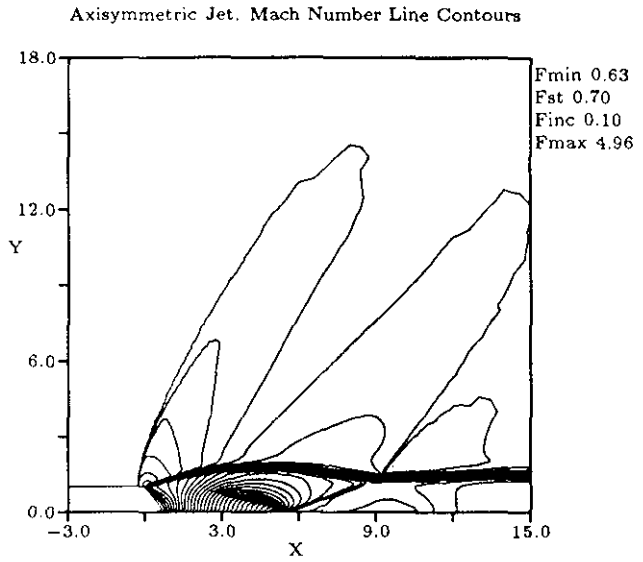

Figure 10: Mach Number Contours, $P_{0_{jet}}/P_{0_{stream}} = 5$, $M = 1.25$

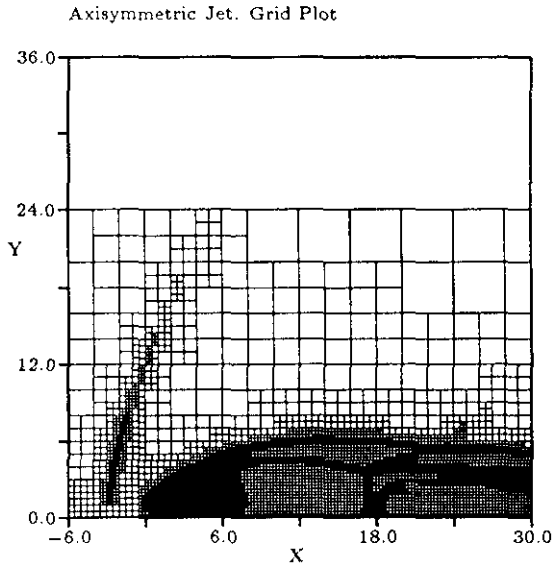

Figure 11: Mesh, $P_{0_{jet}}/P_{0_{stream}} = 50$, $M = 1.25$

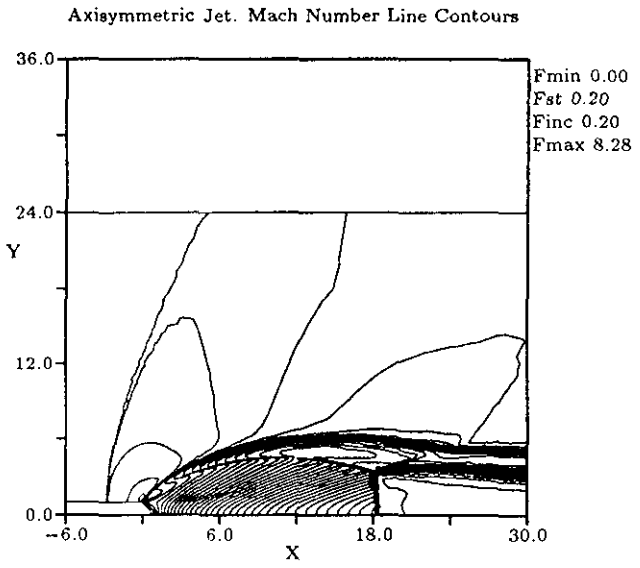

Figure 12: Mach Number Contours, $P_{0_{jet}}/P_{0_{stream}} = 50$, $M = 1.25$

3.4 Total Pressure Ratio of 50, M=1.05

The effect of lowering the Mach number of the jet and the flow is shown in Figures 13 and 14. The results are qualitatively very similar to the previous case, but the Mach disk has weakened, and moved closer to the exit of the nozzle. Again, the mesh refinement has captured the dominant features of the flow.

4 Concluding Remarks

Because of the isolated regions of high gradient, under-expanded jet flows are most efficiently calculated by adaptive procedures. Designing a refinement criterion that detects the shocks, the expansions, and the jet boundary is not straightforward, however. The scheme presented in this paper deals with the strong shocks that occur in these flows, and captures the disparate-strength features well. The resulting flows show complex shock/shear/expansion structures, with Mach disks forming at high total-pressure ratios, and the position of the Mach disk sensitive to the Mach number of the jet.

References

[Bar90] T. J. Barth. On unstructured grids and solvers. In *Computational Fluid Dynamics.* Von Kármán Institute for Fluid Dynamics, Lecture Series 1990-04, 1990.

[DP91] D. De Zeeuw and K. G. Powell. An adaptively-refined carterian mesh solver for the Euler equations. To appear in *Journal of Computational Physics*, 1991.

[PPD92] H. Paillère, K. G. Powell, and D. L. De Zeeuw. A wave-model-based refinement criterion for adaptive-grid computation of compressible flows. AIAA Paper 92-0322, 1992.

[T. 64] T. C. Adamson, Jr. The structure of the rocket exhaust plume without reaction at various altitudes. In *Supersonic Flow, Chemical Processes and Radiative Transfer.* Pergamon Press, 1964.

[Tai90] C.-H. Tai. *Acceleration Techniques for Explicit Euler Codes.* PhD thesis, University of Michigan, 1990.

[vL79] B. van Leer. Towards the ultimate conservative difference scheme. V. A second-order sequel to Godunov's method. *Journal of Computational Physics*, 32, 1979.

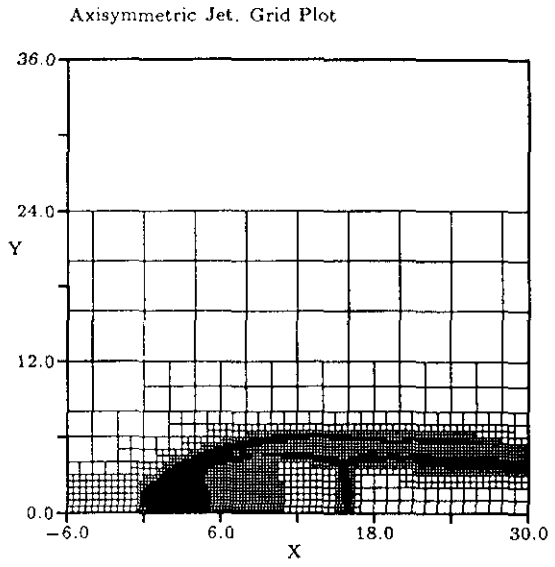

Figure 13: Mesh, $P_{0_{jet}}/P_{0_{stream}} = 50$, $M = 1.05$

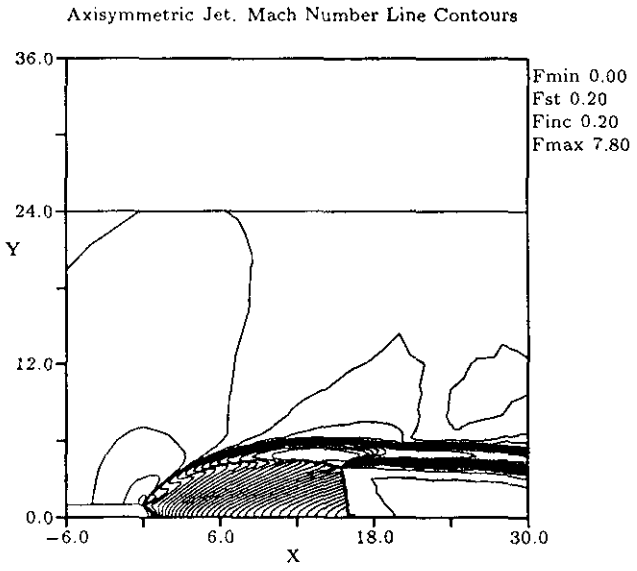

Figure 14: Mach Number Contours, $P_{0_{jet}}/P_{0_{stream}} = 50$, $M = 1.05$

[vLTP89] B. van Leer, C. H. Tai, and K. G. Powell. Design of optimally-smoothing multi-stage schemes for the Euler equations. In *AIAA 9th Computational Fluid Dynamics Conference*, 1989.